IOPscience iopscience.iop.org

Home Search Collections Journals About Contact us My IOPscience

Decoherence of excitonic qubits in Förster coupled quantum dots

This article has been downloaded from IOPscience. Please scroll down to see the full text article.

2008 J. Phys.: Condens. Matter 20 315205

(http://iopscience.iop.org/0953-8984/20/31/315205)

View the table of contents for this issue, or go to the journal homepage for more

Download details:
IP Address: 129.252.86.83
The article was downloaded on 29/05/2010 at 13:47

Please note that terms and conditions apply.

IOP PUBLISHING JOURNAL OF PHYSICS: CONDENSED MATTER

J. Phys.: Condens. Matter **20** (2008) 315205 (9pp) doi:10.1088/0953-8984/20/31/315205

Decoherence of excitonic qubits in Förster coupled quantum dots

A Thilagam and M A Lohe

Department of Physics, The University of Adelaide, 5005, Australia

E-mail: Max.Lohe@adelaide.edu.au

Received 24 April 2008, in final form 25 June 2008
Published 17 July 2008
Online at stacks.iop.org/JPhysCM/20/315205

Abstract

We investigate phonon-assisted mechanisms which contribute to the decoherence of excitonic qubits in quantum dot systems coupled by a Förster-type transfer process. Using the Fermi Golden Rule, we derive explicit expressions for the relaxation and dephasing times for excitonic qubits interacting with acoustic phonons via both the deformation potential and piezoelectric coupling. The decoherence times computed using the Fermi Golden Rule are consistent with those estimated using Bloch–Redfield theory at interdot tunnelling energies small enough for Markovian theories to be valid. Our results show that renormalization of interdot tunnelling frequencies due to phonon interactions is influenced mainly by bias and lattice temperature in GaAs/AlGaAs quantum dot systems.

1. Introduction

Excitons (electron–hole correlated states) in quantum dots are of interest in the solid-state implementation of quantum logic gates [1–4]. Significant advances in creating and probing excitonic states in quantum dots [5, 6] and newly developed techniques, which allow quantum coupling between excitonic states to be continuously varied by external electric fields [4], have provided rapid progress in the field of solid-state quantum computation. For the case of two coupled quantum dot systems, exciton–exciton dipole interactions give rise to diagonal terms which allow quantum logic to be performed via ultra-fast laser pulses on time scales less than the calculated decoherence times [2]. Related studies [7–9] have demonstrated the importance of Förster energy transfers in producing entangled excitonic states, and of using external electric fields to achieve critical logic gate actions. Dipole–dipole interactions were first proposed by Förster [10] and further extended by Dexter [11] as a mechanism of energy transfer for non-overlapping excitonic wavefunctions localized at different lattice sites.

Decoherence due to environmental factors such as phonons and impurities is inevitable and is a major drawback in solid-state devices. Several strategies such as decoherence-free subspaces [12], optimal control techniques [13] and immunization processes [14] have been proposed to counter the detrimental effects of decoherence. It is not immediately clear, however, whether these proposals invoke other routes which facilitate decoherence and, if so, the role played by various system parameters in minimizing errors during logic gate operations. Hence, there is a need to scrutinize the various intrinsic processes, and in particular those that are phonon induced in order to achieve fault tolerant quantum switches.

The interaction of charge carriers with acoustic phonons arises mainly from the deformation potential and piezoelectric coupling in quantum dots [15]. Theoretical estimates by Fedichkin *et al* [16] show that the error rate due to acoustic phonons may be a major factor limiting qubit performance, in agreement with experimental results [17] for a qubit system implemented using a double-dot GaAs/AlGaAs system with a two-dimensional electron gas. Electron–phonon interactions, leading to the formation of polarons [18], are significant in GaAs/InAs quantum dots as compared to bulk systems of the same material. In recent work, Vorojtsov *et al* [20] have studied the role of piezoelectric phonons in qubit systems but without including the Förster coupling mechanism or excitonic interactions. Here we extend the Markovian Bloch–Redfield theory [19], used in [20], to excitonic qubits interacting with acoustic phonons via both the deformation potential and piezoelectric coupling. In order to obtain explicit results, we consider the specific case of excitonic qubits in Förster coupled quantum dots [8]. Earlier work [9] has examined the coupling of the Förster coupled quantum dot system to the external environment consisting of a single radiation mode and associated spontaneous emission and decay processes.

It is not immediately clear whether decoherence phenomena are dominated by relaxation or by pure dephasing processes, and the extent to which the outcome is affected by the

 © 2008 IOP Publishing Ltd Printed in the UK

nature of qubit–phonon coupling during a cycle of logic gate operations. There is a subtle difference between relaxation and pure dephasing of entangled systems. While relaxation leads to shifts in the population of qubit states with one state favoured over another, pure dephasing results in changes in the energy difference between qubit states with the population of qubit states remaining intact. While both processes lead to decoherence of the entangled system, we investigate here the various parameters affecting these two inherent sources of dissipation. We employ the Fermi Golden Rule as well as Markovian Bloch–Redfield theory which provides analytical expressions for the dephasing and relaxation rates [19]. By comparison of decoherence times between the two methods, we study the range of system parameters for which the Fermi Golden Rule yields reliable results for relaxation and pure dephasing times in GaAs/AlGaAs quantum dot systems.

The paper is organized as follows. In section 2 we introduce the model of excitonic qubits in quantum dots and in section 3 derive the explicit expression for the interdot Förster tunnelling amplitude F. In section 4 we examine the different processes that lead to pure dephasing and relaxation of qubit systems interacting with phonons and in section 5 we evaluate matrix elements associated with qubit–phonon interactions via both the deformation potential and piezoelectric coupling. We obtain explicit expressions for the relaxation and dephasing times for excitonic qubits interacting with acoustic phonons in section 6 and provide numerical results for the case of the GaAs/AlGaAs material system. In section 7, we compare results obtained via the Fermi Golden Rule with those of the Markovian Bloch–Redfield theory, followed by conclusions in section 8.

2. Excitonic qubits in quantum dots

We consider two excitons in their ground states in adjacent coupled quantum dots located at $\boldsymbol{R}_a$ and $\boldsymbol{R}_b$. We assume the quantum dots to be shaped in the form of either cuboid boxes or quasi-two-dimensional disks in which the vertical confinement energies of charge carriers are larger than their lateral confinement energies. We label the localized excitonic states as $|\boldsymbol{R}_a\rangle$ and $|\boldsymbol{R}_b\rangle$. In the notation of our earlier work [21], we represent $|\boldsymbol{R}_a\rangle$ according to

$$|\boldsymbol{R}_a\rangle = \frac{v_0}{L}\sum_{\boldsymbol{r}_\mathrm{e},\boldsymbol{r}_\mathrm{h}} \Phi(\boldsymbol{R}_a, \boldsymbol{r}_{\mathrm{e}\parallel}, \boldsymbol{r}_{\mathrm{h}\parallel}, z_\mathrm{e}, z_\mathrm{h})\, a^\dagger_{c,\boldsymbol{r}_\mathrm{e}} a_{v,\boldsymbol{r}_\mathrm{h}} |\boldsymbol{0}\rangle, \qquad (1)$$

where v_0 is the volume of the unit cell, L is the quantization length and $a^\dagger_{c,\boldsymbol{r}_\mathrm{e}}$ ($a_{v,\boldsymbol{r}_\mathrm{h}}$) is the creation (annihilation) operator of an electron in the conduction (valence) band, denoted by c (v). $|\boldsymbol{0}\rangle$ denotes the electronic state of the quantum dot in which all electronic ground states are occupied and all excited states are unoccupied. For simplicity we ignore spin effects, as exchange interactions due to singlet excitons are generally very small [22]. The position vectors $\boldsymbol{r}_\mathrm{e}$ and $\boldsymbol{r}_\mathrm{h}$ may be decomposed into components parallel and perpendicular to the lateral direction of the quantum dot according to $\boldsymbol{r}_\mathrm{e} = (\boldsymbol{r}_{\mathrm{e}\parallel}, z_\mathrm{e})$ and $\boldsymbol{r}_\mathrm{h} = (\boldsymbol{r}_{\mathrm{h}\parallel}, z_\mathrm{h})$. The vertical confinement energies of charge carriers are assumed to be larger than the lateral confinement energies, and therefore we may factorize the exciton wavefunction Φ according to

$$\Phi(\boldsymbol{R}_a, \boldsymbol{r}_{\mathrm{e}\parallel}, \boldsymbol{r}_{\mathrm{h}\parallel}, z_\mathrm{e}, z_\mathrm{h}) = \Psi(\boldsymbol{R}_a, \boldsymbol{r}_{\mathrm{e}\parallel}, \boldsymbol{r}_{\mathrm{h}\parallel})\varphi_\mathrm{e}(z_\mathrm{e})\varphi_\mathrm{h}(z_\mathrm{h}), \qquad (2)$$

where $\varphi_\mathrm{e}(z_\mathrm{e})$ ($\varphi_\mathrm{h}(z_\mathrm{h})$) is the envelope function of the electron (hole) in the vertical direction of the quantum dot. The form of the in-plane exciton wavefunction $\Psi(\boldsymbol{R}_a, \boldsymbol{r}_{\mathrm{e}\parallel}, \boldsymbol{r}_{\mathrm{h}\parallel})$ at $\boldsymbol{R}_a$ depends on the degree of confinement of the electron–hole within the quantum dot. We consider a strong individual charge carrier regime in which the kinetic motions of the electrons and holes are quantized separately, so that the resulting discrete energy levels are affected by the Coulomb interaction between the electron and hole by only a small amount, of the order ℓ^{-1} where ℓ is the quantum dot radius.

$\Psi(\boldsymbol{R}_a, \boldsymbol{r}_{\mathrm{e}\parallel}, \boldsymbol{r}_{\mathrm{h}\parallel})$ may be further factorized by the following change of coordinates:

$$\boldsymbol{r}_\parallel = \frac{1}{\ell_r}(\boldsymbol{r}_{\mathrm{e}\parallel} - \boldsymbol{r}_{\mathrm{h}\parallel}), \qquad \boldsymbol{R} = \frac{1}{\ell_r^2}(\ell_\mathrm{h}^2\, \boldsymbol{r}_{\mathrm{e}\parallel} - \ell_\mathrm{e}^2\, \boldsymbol{r}_{\mathrm{h}\parallel}),$$

where $\ell_r = \sqrt{\ell_\mathrm{e}^{\,2} + \ell_\mathrm{h}^{\,2}}$. The effective lengths ℓ_e and ℓ_h are related to the respective electron and hole effective masses and confining potential frequencies ω_0^e and ω_0^h by $\ell_\mathrm{e} = \sqrt{\frac{\hbar}{m_\mathrm{e}\omega_0^\mathrm{e}}}$ and $\ell_\mathrm{h} = \sqrt{\frac{\hbar}{m_\mathrm{h}\omega_0^\mathrm{h}}}$. We may now write Ψ in the factorized form $\Psi(\boldsymbol{R}_a, \boldsymbol{r}_{\mathrm{e}\parallel}, \boldsymbol{r}_{\mathrm{h}\parallel}) = \Xi(\boldsymbol{R}, \boldsymbol{R}_a)\ \psi(\boldsymbol{r}_\parallel)$ where the confining potential in the lateral direction is modelled using harmonic potentials, so that ψ, Ξ take the form:

$$\begin{aligned} \psi(\boldsymbol{r}_\parallel) &= \frac{1}{\sqrt{\pi}\ell_r}\exp\left(-\frac{r_\parallel^2}{2\ell_r^{\,2}}\right), \\ \Xi(\boldsymbol{R}, \boldsymbol{R}_a) &= \frac{1}{\sqrt{\pi}L_R}\exp\left(-\frac{1}{2L_R^{\,2}}|\boldsymbol{R}_\parallel - \boldsymbol{R}_a|^2\right) \end{aligned} \qquad (3)$$

where $L_R = \ell_\mathrm{e}\ell_\mathrm{h}/\ell_r$. The length scales ℓ_e and ℓ_h associated with the harmonic potential are smaller than the effective Bohr radius of the exciton due to strong confinement of charge carriers in the quantum dot. Due to the Gaussian form of Ξ we can obtain an explicit expression for the two-dimensional Fourier transform $\widetilde{\Xi}$:

$$\begin{aligned} \Xi(\boldsymbol{R}, \boldsymbol{R}_a) &= \int \mathrm{d}^2\boldsymbol{q}_\parallel\ \exp(\mathrm{i}\boldsymbol{q}_\parallel \cdot \boldsymbol{R})\ \ \widetilde{\Xi}(\boldsymbol{q}_\parallel, \boldsymbol{R}_a), \\ \widetilde{\Xi}(\boldsymbol{q}_\parallel, \boldsymbol{R}_a) &= \frac{L_R}{2\pi\sqrt{\pi}}\exp\left(-\mathrm{i}\boldsymbol{q}_\parallel \cdot \boldsymbol{R}_a - \frac{1}{2}L_R^{\,2}q_\parallel^2\right). \end{aligned} \qquad (4)$$

The confining potential in the vertical direction is modelled using harmonic potentials defined by the vertical confinement dimensions $\ell_{z\mathrm{e}}$ and $\ell_{z\mathrm{h}}$ for electrons and holes respectively, leading to the wavefunctions:

$$\begin{aligned} \varphi_\mathrm{e}(z_\mathrm{e}) &= \left(\frac{1}{\sqrt{\pi}\ell_{z\mathrm{e}}}\right)^{1/2}\exp\left(-\frac{z_\mathrm{e}^2}{2\ell_{z\mathrm{e}}^{\,2}}\right), \\ \varphi_\mathrm{h}(z_\mathrm{h}) &= \left(\frac{1}{\sqrt{\pi}\ell_{z\mathrm{h}}}\right)^{1/2}\exp\left(-\frac{z_\mathrm{h}^2}{2\ell_{z\mathrm{h}}^{\,2}}\right). \end{aligned} \qquad (5)$$

The excitonic state $|\boldsymbol{R}_b\rangle$ is analogous in form to equation (1).

We code the excitonic qubits states using the relative position of the exciton via the basis set $\{|\boldsymbol{L}\rangle, |\boldsymbol{R}\rangle\}$:

$$|\boldsymbol{L}\rangle = |\boldsymbol{R}_a\rangle \otimes |\boldsymbol{0}\rangle_b, \qquad |\boldsymbol{R}\rangle = |\boldsymbol{0}\rangle_a \otimes |\boldsymbol{R}_b\rangle, \tag{6}$$

where the states $|\boldsymbol{0}\rangle_a$ and $|\boldsymbol{0}\rangle_b$, which correspond to the absence of excitons, denote the respective ground states of the quantum dots at $|\boldsymbol{R}_a\rangle$ and $|\boldsymbol{R}_b\rangle$. We simplify this approach by considering a two-level system involving only the states $|\boldsymbol{L}\rangle$ and $|\boldsymbol{R}\rangle$, and work in the limit of a pure Förster coupling. The direct Coulomb interaction, which causes the formation of the biexciton state $|\boldsymbol{R}_a\rangle|\boldsymbol{R}_b\rangle$, is neglected and we also exclude the possibility of entangled states involving the vacuum state $|\boldsymbol{0}\rangle_a|\boldsymbol{0}\rangle_b$. The two-level excitonic qubit Hamiltonian takes the form

$$\widehat{H}_{\mathrm{ex-qb}} = -\hbar\left(\frac{\Delta\Omega}{2}\sigma_z + F\,\sigma_x\right), \tag{7}$$

where the Pauli matrices are given by $\sigma_x = |\boldsymbol{L}\rangle\langle\boldsymbol{R}| + |\boldsymbol{R}\rangle\langle\boldsymbol{L}|$ and $\sigma_z = |\boldsymbol{L}\rangle\langle\boldsymbol{L}| - |\boldsymbol{R}\rangle\langle\boldsymbol{R}|$, and $\Delta\Omega = \Omega_a - \Omega_b$ denotes the difference in exciton creation energy between the quantum dot at $\boldsymbol{R}_a$ and that at $\boldsymbol{R}_b$ and can be regarded as the biasing energy. F denotes the interdot Förster tunnelling amplitude responsible for the transfer of an exciton from one quantum dot to the other without involving a physical tunnelling process.

The symmetric and antisymmetric eigenstates of this interacting qubit system are given by

$$\begin{aligned} |\chi_{\mathrm{s}}\rangle &= \cos\frac{\beta}{2}|\boldsymbol{L}\rangle \ + \sin\frac{\beta}{2}|\boldsymbol{R}\rangle \\ |\chi_{\mathrm{as}}\rangle &= \sin\frac{\beta}{2}|\boldsymbol{L}\rangle \ - \cos\frac{\beta}{2}|\boldsymbol{R}\rangle, \end{aligned} \tag{8}$$

with corresponding energies

$$E_{\mathrm{as(s)}} = \Omega_0 + \Omega_a - \frac{\Delta\Omega}{2} \pm \sqrt{\left(\frac{\Delta\Omega}{2}\right)^2 + F^2}, \tag{9}$$

where Ω_0 denotes the ground state energy of the system in which each quantum dot is unoccupied by excitons. The energy difference between the eigenstates is $\sqrt{\Delta\Omega^2 + (2F)^2}$ and can be studied as a function of time. In the absence of any decoherence, the excitonic qubit oscillates coherently between the two dots with the Rabi frequency $E_{\mathrm{as}} - E_{\mathrm{s}}$. The polar angle β in the Bloch sphere representation of a qubit is related to $\Delta\Omega$ and F by $\tan\beta = \frac{2F}{\Delta\Omega}$.

3. Interdot Förster tunnelling amplitude F

The concept of Förster resonance energy transfer has been applied successfully to the description of nonradiative transitions in quantum dot systems and has been shown to be reliable when applied to semiconductor nanocrystals [23]. When the distance between two quantum dots is larger than the quantum dot sizes and the excitons are well localized, the electronic states of the quantum dots become coupled by long-range Coulomb interactions.

The magnitude of the interdot Förster tunnelling amplitude F is determined from (Dexter [11]):

$$\begin{aligned} F &= \langle\boldsymbol{R}|\widehat{H}_{\mathrm{F}}|\boldsymbol{L}\rangle \\ &= \sum_{r_a, r_b} \langle g, \boldsymbol{R}_a;\, f, \boldsymbol{R}_b|U(|\boldsymbol{r}_a - \boldsymbol{r}_b|)|f, \boldsymbol{R}_a;\, g, \boldsymbol{R}_b\rangle \\ &\quad + \sum_{r_a, r_b} \langle g, \boldsymbol{R}_a;\, f, \boldsymbol{R}_b|U(|\boldsymbol{r}_a - \boldsymbol{r}_b|)|g, \boldsymbol{R}_b;\, f, \boldsymbol{R}_a\rangle, \end{aligned} \tag{10}$$

where the Förster Hamiltonian $\widehat{H}_{\mathrm{F}}$, which is included in the Hamiltonian $\widehat{H}_{\mathrm{ex-qb}}$ in equation (7), is given by

$$\widehat{H}_{\mathrm{F}} = -\hbar F\,\sigma_x, \tag{11}$$

and $U(|\boldsymbol{r}_a - \boldsymbol{r}_b|) = e^2/(\epsilon\,|\boldsymbol{r}_a - \boldsymbol{r}_b|)$, where $\boldsymbol{r}_a$ and $\boldsymbol{r}_b$ are the position vectors of the charge carriers with origins at the centre of the quantum dots located at $\boldsymbol{R}_a$ and $\boldsymbol{R}_b$ respectively. The background dielectric constant is $\epsilon = \epsilon_0\,\epsilon_{\mathrm{r}}$ where the relative permittivity ϵ_{r} is assumed to be independent of the location of charge carriers. We assume that an incident photon of appropriate energy excites the electronic state of the crystal such that an electron is excited in the electronic state f and a hole is excited in the ground state g. Therefore f and g denote the respective energy levels of the electron and hole with respect to the ground state of the crystal where the valence band is completely occupied and the conduction band is unoccupied. In the two-particle interaction matrix element

$$\langle g, \boldsymbol{R}_a;\, f, \boldsymbol{R}_b|U(|\boldsymbol{r}_a - \boldsymbol{r}_b|)|f, \boldsymbol{R}_a;\, g, \boldsymbol{R}_b\rangle,$$

the states to the right of the scattering potential U represent the initial states while those to the left represent the final scattered states. The first matrix element on the right-hand side of equation (10) is due to the Coulomb interaction in which the excited electron, in its initial state f in the quantum dot at $\boldsymbol{R}_a$, and a hole in the state g in the quantum dot at $\boldsymbol{R}_b$, are scattered through the potential U to final states in which the electron and hole remain in the same excited states but with exchanged positions. The net effect can be viewed as a tunnelling process in which the exciton is physically transferred from one quantum dot to another. The second matrix element in equation (10) represents the scattering of an electron, in its initial state f in the quantum dot at $\boldsymbol{R}_a$, and a hole in the state g in the quantum dot at $\boldsymbol{R}_b$, through the potential U such that they remain at their respective quantum dot sites but with exchanged excited states. This second process can be viewed as one in which the excited electron in one quantum dot recombines with the hole in the ground state, and the liberated energy is then transferred to excite the electron–hole pair in a neighbouring quantum dot. We assume that the quantum dots are separated by a distance $W = |\boldsymbol{R}_a - \boldsymbol{R}_b|$ such that $W \gg |\boldsymbol{r}_a - \boldsymbol{r}_b|$, so that tunnelling effects are negligible. The interdot Förster energy transfer is then determined by the second matrix element in equation (10).

By substituting the expressions for $|\boldsymbol{R}_a\rangle$ and $|\boldsymbol{R}_b\rangle$ (given by equation (1)) into equation (10) and by employing the Förster multipole expansion of the Coulomb interaction we

obtain:

$$\langle \boldsymbol{R}|\widehat{H}_{\rm F}|\boldsymbol{L}\rangle = \frac{\upsilon_0^2}{4\pi\epsilon|\boldsymbol{R}_a-\boldsymbol{R}_b|^3} \times \sum_{\boldsymbol{r}_{\rm e},\boldsymbol{r}_{\rm h}}\sum_{\boldsymbol{r}'_{\rm e},\boldsymbol{r}'_{\rm h}} \Psi(\boldsymbol{R}_a,\boldsymbol{r}_{\rm e\|},\boldsymbol{r}_{\rm h\|})\Psi^*(\boldsymbol{R}_b,\boldsymbol{r}'_{\rm e\|},\boldsymbol{r}'_{\rm h\|}) \times \varphi_{\rm e}(z_{\rm e})\,\varphi_{\rm h}(z_{\rm h})\,\varphi^*_{\rm e}(z'_{\rm e})\,\varphi^*_{\rm h}(z'_{\rm h}) \times \left[\boldsymbol{\mu}_a\cdot\boldsymbol{\mu}_b - 3(\boldsymbol{\mu}_a\cdot\boldsymbol{R}_d)(\boldsymbol{\mu}_b\cdot\boldsymbol{R}_d)\right]\,\delta_{\boldsymbol{r}_{\rm e},\boldsymbol{r}_{\rm h}}\,\delta_{\boldsymbol{r}'_{\rm e},\boldsymbol{r}'_{\rm h}}, \quad (12)$$

where $\boldsymbol{R}_d = \frac{\boldsymbol{R}_a-\boldsymbol{R}_b}{|\boldsymbol{R}_a-\boldsymbol{R}_b|}$, and

$$\boldsymbol{\mu}_{a(b)} = \int u_c(\boldsymbol{r})\,(\boldsymbol{r}_{a(b)}-\boldsymbol{r})\,u_v(\boldsymbol{r})\,{\rm d}\boldsymbol{r}, \quad (13)$$

where $u_c(\boldsymbol{r})$ and $u_v(\boldsymbol{r})$ are the respective periodic components of the bulk Bloch functions of the electron and hole. We assume that the Bloch functions are identical in both the quantum dot and barrier materials.

Using equations (3)–(5) in equation (12), we obtain:

$$F(W) = \langle \boldsymbol{R}|\widehat{H}_{\rm F}|\boldsymbol{L}\rangle = \sqrt{\frac{11}{8}}\frac{\boldsymbol{\mu}\cdot\boldsymbol{\mu}}{\epsilon W^3}\left(\frac{2\ell_{\rm e}\ell_{\rm h}}{\ell_{\rm e}^{\,2}+\ell_{\rm h}^{\,2}}\right)^2\left(\frac{2\ell_{z\rm e}\ell_{z\rm h}}{\ell_{z\rm e}^{\,2}+\ell_{z\rm h}^{\,2}}\right), \quad (14)$$

where $\boldsymbol{\mu}=\boldsymbol{\mu}_a\simeq\boldsymbol{\mu}_b$ and $W=|\boldsymbol{R}_a-\boldsymbol{R}_b|$. From equation (8) we obtain

$$\langle\chi_{\rm s}|\widehat{H}_F|\chi_{\rm s}\rangle = -\langle\chi_{\rm as}|\widehat{H}_F|\chi_{\rm as}\rangle = \sin\beta\;F(W), \qquad \langle\chi_{\rm as}|\widehat{H}_F|\chi_{\rm s}\rangle = -\cos\beta\;F(W). \quad (15)$$

In view of the fact that F gives rise to the entangled states $|\chi_{\rm s}\rangle$ and $|\chi_{\rm as}\rangle$, we expect the inevitable loss of energy to lattice vibrations coupled with the excitation transfer to lead to decoherence and subsequent degradation of qubit states. We investigate this important process in greater detail in the next section.

4. Excitonic qubit–phonon interaction

We consider the exciton state at each quantum dot to be coupled to a continuum of acoustic phonons via both the deformation potential and piezoelectric coupling. The acoustic phonons are modelled as bulk modes which is a valid approximation for quantum dots fabricated in barrier materials with similar lattice properties, such as (In,Ga)As quantum dots with a (Ga, Al)As barrier. The total Hamiltonian $\widehat{H}^{\rm env}_{\rm qb}$ of a system of Förster coupled quantum dots interacting with phonons is given by

$$\widehat{H}^{\rm env}_{\rm qb} = \widehat{H}_{\rm ex-qb} + \widehat{H}^{\rm ph} + \widehat{H}^{\rm DP}_{\rm ex-qb} + \widehat{H}^{\rm Piez}_{\rm ex-qb,\lambda} + \widehat{H}^{\rm ph}_{\rm F}, \quad (16)$$

each term of which we now explain in turn. $\widehat{H}_{\rm ex-qb}$ is given by equation (7), $\widehat{H}^{\rm ph}$ denotes the Hamiltonian for the phonon bath

$$\widehat{H}_{\rm ph} = \sum_{\boldsymbol{q}}\hbar\omega_{q,\lambda}b^\dagger_\lambda(\boldsymbol{q})b_\lambda(\boldsymbol{q}), \quad (17)$$

where $b^\dagger_\lambda(\boldsymbol{q})$, and $b_\lambda(\boldsymbol{q})$, are the respective creation and annihilation operators of a λ-mode phonon with wavevector $\boldsymbol{q}$. The λ-mode is denoted LA for longitudinal acoustic phonons and TA for transverse acoustic phonons. The acoustic phonon energy spectrum is determined by the dispersion relation $\omega_{q,\rm LA}=\upsilon_{\rm LA}|\boldsymbol{q}|$ for the longitudinal mode and $\omega_{q,\rm TA}=\upsilon_{\rm TA}|\boldsymbol{q}|$ for the transverse mode, with $\upsilon_{\rm LA}$ and $\upsilon_{\rm TA}$ denoting the corresponding sound velocities.

$\widehat{H}^{\rm DP}_{\rm ex-qb}$ denotes the Hamiltonian describing the qubit–phonon interaction via the deformation potential coupling and is linear in terms of phonon creation and annihilation operators:

$$\widehat{H}^{\rm DP}_{\rm ex-qb} = \sum_{\lambda,\boldsymbol{q}}\sqrt{\frac{\hbar|\boldsymbol{q}|^2}{2\rho\,V\,\omega_{q,\lambda}}}\;\left[M_r\,\sigma_x + M_p\,\sigma_z\right] \times \left(b^\dagger_\lambda(-\boldsymbol{q})+b_\lambda(\boldsymbol{q})\right)\;|n_{q,\lambda}\rangle\langle n_{q,\lambda}|, \quad (18)$$

where $|n_{q,\lambda}\rangle$ denotes the occupation number of a λ-mode phonon with wavevector $\boldsymbol{q}$. V is the crystal volume and ρ is the mass density of the material system. $D_{\rm c}$ and $D_{\rm v}$ are the respective deformation potential constants for the conduction and valence bands. The terms M_r and M_p have the expressions

$$M_r = \langle\chi_{\rm as};n_{q,\lambda}\;\pm\;1|\left(D_{\rm c}{\rm e}^{{\rm i}\,\boldsymbol{q}\cdot\boldsymbol{r}_{\rm e}} - D_{\rm v}{\rm e}^{{\rm i}\,\boldsymbol{q}\cdot\boldsymbol{r}_{\rm h}}\right)|\chi_{\rm s};n_{q,\lambda}\rangle,$$
$$M_p = \langle\chi_{\rm s};n_{q,\lambda}\;\pm\;1|\left(D_{\rm c}{\rm e}^{{\rm i}\,\boldsymbol{q}\cdot\boldsymbol{r}_{\rm e}} - D_{\rm v}{\rm e}^{{\rm i}\,\boldsymbol{q}\cdot\boldsymbol{r}_{\rm h}}\right)|\chi_{\rm s};n_{q,\lambda}\rangle - \langle\chi_{\rm as};n_{q,\lambda}\;\pm\;1|\left(D_{\rm c}{\rm e}^{{\rm i}\,\boldsymbol{q}\cdot\boldsymbol{r}_{\rm e}} - D_{\rm v}{\rm e}^{{\rm i}\,\boldsymbol{q}\cdot\boldsymbol{r}_{\rm h}}\right)|\chi_{\rm as};n_{q,\lambda}\rangle.$$

The term involving M_r in the Hamiltonian describes decoherence in which the qubit state $|\chi_{\rm s}\rangle$ relaxes to the state $|\chi_{\rm as}\rangle$ due to mediation by phonons. During this process, phonons disrupt the coherent oscillation between antisymmetric and symmetric states as absorption of phonons elevates the symmetric state to an antisymmetric state of higher energy. The M_p term describes a second type of decoherence in which a shift occurs in the energy difference between the two qubit states resulting in pure dephasing of the entangled system.

An expression similar to equation (18) can be obtained for the Hamiltonian $\widehat{H}^{\rm Piez}_{\rm ex-qb,\lambda}$ describing exciton–phonon interactions via piezoelectric coupling:

$$\widehat{H}^{\rm Piez}_{\rm ex-qb,\lambda} = \sum_{\lambda,\boldsymbol{q}}\frac{8\pi e e_{14}}{\epsilon_0\epsilon_{\rm r}|\boldsymbol{q}|^2}\sqrt{\frac{\hbar}{2\rho\,V\,\omega_{q,\lambda}}} \times \left(\xi_{x,\lambda}q_yq_z+\xi_{y,\lambda}q_xq_z+\xi_{z,\lambda}q_xq_y\right) \times \left[N_r\,\sigma_x+N_p\,\sigma_z\right]\left(b^\dagger_\lambda(-\boldsymbol{q})+b_\lambda(\boldsymbol{q})\right)\;|n_{q,\lambda}\rangle\langle n_{q,\lambda}|, \quad (19)$$

where the relative permittivity $\epsilon_{\rm r}$ is assumed to be unaffected by the contribution from strain fields associated with acoustic phonon modes. e_{14} denotes the piezoelectric constant and $\xi_{i,\lambda}$ is the unit vector of polarization of the λ-phonon along the i-direction. Excitonic interactions with phonons due to piezoelectric coupling are highly anisotropic in nature [21] and the form of $\widehat{H}^{\rm Piez}_{\rm ex-qb,\lambda}$ depends on the choice of polarization components and on the modes associated with λ. Further details of the dependency on LA, TA1 and TA2 modes are given in the next section. N_r and N_p are defined analogously to M_r and M_p as in equation (19):

$$N_r = \langle\chi_{\rm as};n_{q,\lambda}\pm1|\left({\rm e}^{{\rm i}\,\boldsymbol{q}\cdot\boldsymbol{r}_{\rm e}}-{\rm e}^{{\rm i}\,\boldsymbol{q}\cdot\boldsymbol{r}_{\rm h}}\right)|\chi_{\rm s};n_{q,\lambda}\rangle,$$
$$N_p = \langle\chi_{\rm s};n_{q,\lambda}\pm1|\left({\rm e}^{{\rm i}\,\boldsymbol{q}\cdot\boldsymbol{r}_{\rm e}}-{\rm e}^{{\rm i}\,\boldsymbol{q}\cdot\boldsymbol{r}_{\rm h}}\right)|\chi_{\rm s};n_{q,\lambda}\rangle - \langle\chi_{\rm as};n_{q,\lambda}\pm1|\left({\rm e}^{{\rm i}\,\boldsymbol{q}\cdot\boldsymbol{r}_{\rm e}}-{\rm e}^{{\rm i}\,\boldsymbol{q}\cdot\boldsymbol{r}_{\rm h}}\right)|\chi_{\rm as};n_{q,\lambda}\rangle.$$

Unlike M_r or M_p, each of N_r, N_p vanishes as $\boldsymbol{q} \to 0$ due to the exact cancellation of electron and hole form factors, as the piezoelectric coupling constant is the same for electrons and holes.

We consider the Hamiltonian $\widehat{H}_{\rm F}^{\rm ph}$ in equation (16) to be associated with phonon-assisted interactions by which the interdot tunnelling amplitude F becomes dressed by a Franck–Cordon (FC) factor as described in [25]. A brief study of the temperature dependence of F is given in section 7.1 where we show that in materials of weak exciton–phonon interactions, the FC factor can be neglected at low temperatures ($T \sim$ 10–50 K).

5. Evaluation of matrix elements

By using equations (1), (3), (4) and (5) in equation (18) we obtain explicit forms for the matrix elements:

$$\langle \boldsymbol{L}; n_{\boldsymbol{q},\lambda} \pm 1|\widehat{H}_{\rm ex-qb}^{\rm DP}|\boldsymbol{L}; n_{\boldsymbol{q},\lambda}\rangle = \Sigma_D(q_\parallel, q_z)\, {\rm e}^{-{\rm i}\boldsymbol{q}\cdot\boldsymbol{R}_a} \tag{20}$$

$$\langle \boldsymbol{L}; n_{\boldsymbol{q},\lambda} \pm 1|\widehat{H}_{\rm ex-qb}^{\rm DP}|\boldsymbol{R}; n_{\boldsymbol{q},\lambda}\rangle = \Sigma_D(q_\parallel, q_z){\rm e}^{-{\rm i}\boldsymbol{q}\cdot\frac{(\boldsymbol{R}_a+\boldsymbol{R}_b)}{2}}{\rm e}^{-\frac{W^2}{4L_R{}^2}}, \tag{21}$$

where

$$\Sigma_D(q_\parallel, q_z) = \sqrt{\frac{\hbar\,|\boldsymbol{q}|^2}{2\rho\, V\, \omega_{\boldsymbol{q},\lambda}}}{\rm e}^{-\frac{1}{4}L_R{}^2 q_\parallel{}^2} \times \left[D_{\rm c}\ {\rm e}^{-\frac{1}{4}\ell_{\rm ze}{}^2 q_z^2}\ {\rm e}^{-\frac{1}{4}\ell_{\rm e}{}^2 q_\parallel^2} - D_{\rm v}{\rm e}^{-\frac{1}{4}\ell_{\rm zh}{}^2 q_z^2}\ {\rm e}^{-\frac{1}{4}\ell_{\rm h}{}^2 q_\parallel^2}\right], \tag{22}$$

where $L_R = \ell_{\rm e}\ell_{\rm h}/\ell_r$. An expression similar to equation (20) can be obtained for $\langle \boldsymbol{R}; n_{\boldsymbol{q},\lambda} \pm 1|\widehat{H}_{\rm ex-qb}^{\rm DP}|\boldsymbol{R}; n_{\boldsymbol{q},\lambda}\rangle$. The function $\Sigma_D(q_\parallel, q_z)$ differs from the commonly used form [16] as here we consider non-isotropic propagation of phonons. From equations (8), (20) and (21) we obtain

$$\begin{aligned}&\langle \chi_{\rm as}; n_{\boldsymbol{q},\lambda} \pm 1|\widehat{H}_{\rm ex-qb}^{\rm DP}|\chi_{\rm s}; n_{\boldsymbol{q},\lambda}\rangle \\ &= \frac{1}{2}\sin\frac{\beta}{2}\left({\rm e}^{-{\rm i}\boldsymbol{q}\cdot\boldsymbol{R}_a} - {\rm e}^{-{\rm i}\boldsymbol{q}\cdot\boldsymbol{R}_b}\right)\Sigma_D(q_\parallel, q_z) \\ &\quad - \cos\frac{\beta}{2}{\rm e}^{-\frac{W^2}{4L_R{}^2}}\Sigma_D(q_\parallel, q_z).\end{aligned} \tag{23}$$

The first term on the right-hand side contains the coherence factor $({\rm e}^{-{\rm i}\boldsymbol{q}\cdot\boldsymbol{R}_a} - {\rm e}^{-{\rm i}\boldsymbol{q}\cdot\boldsymbol{R}_b})$ which remains effective over large distances between the quantum dots. The second term contains the factor ${\rm e}^{-\frac{W^2}{4L_R{}^2}}$ which is short ranged as it depends on the overlap integral of the exciton wavefunctions in quantum dots located at different sites. By integrating the coherence factor over the polar angle ϕ we obtain

$$\begin{aligned}&\left|\langle \chi_{\rm as}; n_{\boldsymbol{q},\lambda} \pm 1|\widehat{H}_{\rm ex-qb}^{\rm DP}|\chi_{\rm s}; n_{\boldsymbol{q},\lambda}\rangle\right|^2 = 2\pi\,\Sigma_D^2(q_\parallel, q_z) \\ &\quad\times\left[\tfrac{1}{2}\sin^2\beta\,(1 - J_0(q_\parallel W)) + \cos^2\beta\,{\rm e}^{-\frac{W^2}{2L_R{}^2}}\right],\end{aligned} \tag{24}$$

where J_0 denotes a Bessel function of order zero. In order to obtain a tractable form of equation (24) we approximate $J_0(q\,W\sin\theta)$ by taking the angular average (as explained in [24]):

$$\begin{aligned}J_0(q\,W\sin\theta) &\approx \frac{\int\int J_0(q\,W\sin\theta)\sin\theta\,{\rm d}\theta\,{\rm d}\phi}{\int\int \sin\theta\,{\rm d}\theta\,{\rm d}\phi} \\ &= \frac{\sin(q\,W)}{q\,W}.\end{aligned}$$

Hence for large separations W between the quantum dots, we may approximate the matrix element in equation (24) as follows:

$$\begin{aligned}&|\langle \chi_{\rm as}; n_{\boldsymbol{q},\lambda} \pm 1|\widehat{H}_{\rm ex-qb}^{\rm DP}|\chi_{\rm s}; n_{\boldsymbol{q},\lambda}\rangle|^2 \\ &\quad\approx \pi\,\Sigma_D^2(q_\parallel, q_z)\sin^2\beta\left(1 - \frac{\sin q\,W}{q\,W}\right).\end{aligned}$$

Expressions similar to equation (24) but with slight variations in the dependency on the polar angle β can be obtained for $|\langle \chi_{\rm as}; n_{\boldsymbol{q},\lambda} \pm 1|\widehat{H}_{\rm ex-qb}^{\rm DP}|\chi_{\rm as}; n_{\boldsymbol{q},\lambda}\rangle|^2$ and also $|\langle \chi_{\rm s}; n_{\boldsymbol{q},\lambda} \pm 1|\widehat{H}_{\rm ex-qb}^{\rm DP}|\chi_{\rm s}; n_{\boldsymbol{q},\lambda}\rangle|^2$. These expressions are used in the following section, together with equation (19), to evaluate the rates at which the excitonic qubits lose their decoherence via relaxation and dephasing.

For the case of the qubit–phonon interaction via piezoelectric coupling, we choose phonon polarization components with respect to the cubic crystallographic axes of the zinc-blende type crystal. By substituting equations (1), (3), (4) and (5) into equation (19), we obtain the following explicit forms for the matrix elements:

$$\begin{aligned}&\langle \boldsymbol{L}; n_{\boldsymbol{q},\lambda} \pm 1|\widehat{H}_{\rm ex-qb,\lambda}^{\rm Piez}|\boldsymbol{L}; n_{\boldsymbol{q},\lambda}\rangle = \Sigma_P(q_\parallel, q_z, \lambda)\ {\rm e}^{-\boldsymbol{q}_\parallel\cdot\boldsymbol{R}_a} \\ &\langle \boldsymbol{L}; n_{\boldsymbol{q},\lambda} \pm 1|\widehat{H}_{\rm ex-qb,\lambda}^{\rm Piez}|\boldsymbol{R}; n_{\boldsymbol{q},\lambda}\rangle \\ &\quad = \Sigma_P(q_\parallel, q_z, \lambda)\ {\rm e}^{-\boldsymbol{q}_\parallel\cdot\frac{(\boldsymbol{R}_a+\boldsymbol{R}_b)}{2}}{\rm e}^{-\frac{W^2}{4L_R{}^2}},\end{aligned} \tag{25}$$

where

$$\begin{aligned}&\Sigma_P(q_\parallel, q_z, \lambda) \\ &= \frac{4\pi e e_{14}}{\epsilon_0\epsilon_{\rm r}}\sqrt{\frac{\hbar}{2\rho\, V\, \upsilon_\lambda q}}\ A_\lambda(\theta,\phi)\ {\rm e}^{-\frac{1}{4}L_R{}^2 q_\parallel{}^2} \\ &\quad\times\left[{\rm e}^{-\frac{1}{4}\ell_{\rm ze}{}^2 q_z^2}\ {\rm e}^{-\frac{1}{4}\ell_{\rm e}{}^2 q_\parallel^2} - {\rm e}^{-\frac{1}{4}\ell_{\rm zh}{}^2 q_z^2}\ {\rm e}^{-\frac{1}{4}\ell_{\rm h}{}^2 q_\parallel^2}\right].\end{aligned} \tag{26}$$

The anisotropy factor $A_\lambda(\theta,\phi)$ is given [16] by the expressions:

$$A_{\rm LA}(\theta,\phi) = \tfrac{3}{4}\sin 2\theta\sin\theta\sin 2\phi, \tag{27}$$

$$A_{\rm TA1}(\theta,\phi) = \tfrac{1}{8}(\sin\theta - \sin 3\theta)\sin 2\phi, \tag{28}$$

$$A_{\rm TA2}(\theta,\phi) = \tfrac{1}{2}\sin 2\theta\cos 2\phi. \tag{29}$$

The TA1 and TA2 modes correspond to the two possible polarized directions of the transverse phonon. Calculation of $|\langle \chi_{\rm as}; n_{\boldsymbol{q},\lambda} \pm 1|\widehat{H}_{\rm ex-qb,\lambda}^{\rm Piez}|\chi_{\rm s}; n_{\boldsymbol{q},\lambda}\rangle|^2$, where $\lambda =$ LA, TA1, TA2, is more involved due to the presence of the angle ϕ in equations (27)–(29). For $\lambda =$ LA we obtain

$$\begin{aligned}&|\langle \chi_{\rm as}; n_{q,{\rm LA}\pm1}|\widehat{H}_{\rm ex-qb,LA}^{\rm Piez}|\chi_{\rm s}; n_{q,{\rm LA}}\rangle|^2 \\ &= \frac{\pi}{4}\Sigma_P^2(q_\parallel, q_z, {\rm LA}) \\ &\quad\times\left[\sin^2\beta\left(1 - \frac{\sin q\,W}{q\,W}\right) + 9\cos^2\beta{\rm e}^{-\frac{W^2}{2L_R{}^2}}\right],\end{aligned} \tag{30}$$

where $\Sigma_P(q_\parallel, q_z, {\rm LA})$ is obtained using equations (26) and (27). Similar expressions can be obtained for the TA1 and TA2 modes of the transverse phonon using equations (28) and (29).

6. Decoherence rates of excitonic qubits

We employ the Fermi Golden Rule to compute decoherence rates, adhering to the conditions (discussed in chapter 18 of [26]) underlying the perturbation theory from which the Golden Rule is derived. An essential condition is that the interaction time T of the perturbation remain sufficiently long to satisfy $\Delta E \gg \frac{2\pi\hbar}{T}$, where ΔE is the energy range of states involved in the transitions, in which the initial state is not appreciably depleted during the transition period. At low lattice temperatures, small Förster interaction energies and weak exciton–phonon interactions, the decoherence rates associated with relaxation and pure dephasing processes are therefore calculated using

$$\frac{1}{\tau_{\mathrm{X},\lambda}} = \frac{2\pi}{\hbar} \sum_{q_\parallel, q_z} \left|\langle \mathrm{f}|\widehat{H}_{\mathrm{int}}|\mathrm{i}\rangle\right|^2 (N_{q,\lambda}+1)\, \delta(\Delta E \pm \hbar\omega_{q,\lambda}), \quad (31)$$

where the initial and final states $|\mathrm{i}\rangle$ and $|\mathrm{f}\rangle$ are constructed from $|\chi_{\mathrm{as}}; n_{q,\lambda}\rangle$ and $|\chi_{\mathrm{s}}; n_{q,\lambda}\rangle$. ΔE is the energy difference between the initial and final states and determines the wavevector of the emitted phonon. The interaction Hamiltonian $\widehat{H}_{\mathrm{int}}$ is equal to either $\widehat{H}^{\mathrm{DP}}_{\mathrm{ex-qb}}$ or $\widehat{H}^{\mathrm{Piez}}_{\mathrm{ex-qb},\lambda}$ depending on the type of phonon coupling. In the case of decoherence associated with Förster transfer, $\widehat{H}_{\mathrm{int}}$ is given by $\widehat{H}^{\mathrm{ph}}_{\mathrm{F}}$, details of which appear in the next section. $N_{q,\lambda}$ denotes the thermalized average number of phonons at temperature T and is given by the Bose–Einstein distribution $N_{q,\lambda} = [\exp(\hbar\omega_{q,\lambda}/k_{\mathrm{B}}T) - 1]^{-1}$ where k_{B} is the Boltzmann constant.

From equations (19), (24), (31) we obtain explicit expressions for the rate of relaxation $(1/\tau^r_{\mathrm{DP}})$ and for the rate of dephasing $(1/\tau^p_{\mathrm{DP}})$ of excitonic qubits:

$$\frac{1}{\tau^{r(p)}_{\mathrm{DP}}} = \frac{(D_{\mathrm{c}} - D_{\mathrm{v}})^2 q^3}{4\sqrt{\pi}\hbar\rho\upsilon^2_{\mathrm{LA}}} \exp\left(-\frac{3}{4}q^2\ell^2\right) \times \frac{\mathrm{Erfi}(\Delta\ell)}{\Delta\ell}(N_{q,\lambda}+1)S_{r(p)}(\beta), \quad (32)$$

where the functions S_r and S_p are given by

$$S_r(\beta) = \frac{1}{2}\sin^2\beta\left(1 - \frac{\sin qW}{qW}\right) + \cos^2\beta \mathrm{e}^{-\frac{W^2}{\ell^2}},$$
$$S_p(\beta) = \frac{1}{2}\cos^2\beta\left(1 - \frac{\sin qW}{qW}\right) + \frac{1}{2}\sin^2\beta \mathrm{e}^{-\frac{W^2}{\ell^2}}.$$

In order to simplify equation (32) and its derivation, we have assumed that $\ell_{\mathrm{e}} \approx \ell_{\mathrm{h}} = \ell$ and $\ell_{z\mathrm{e}} \approx \ell_{z\mathrm{h}} = \ell_z$. Erfi denotes the imaginary error function, $\Delta\ell = q\sqrt{\frac{1}{2}(\frac{3}{2}\ell^2 - {\ell_z}^2)}$ and $q = \frac{2F(W)}{\hbar\upsilon_{\mathrm{LA}}}\sqrt{1+\gamma^2}$ where $\gamma = \frac{\Delta\Omega}{2F(W)}$ (see equation (14) for an analytical expression for $F(W)$). The tuning factor γ is the ratio of the level asymmetry or bias $(\Delta\Omega)$ to the tunnelling amplitude given by $2F(w)$, where the level asymmetry is determined by the difference in exciton creation energies at the separate quantum dots. Thus γ can be controlled in two ways, first by changing the bias and second by changing $F(W)$. In Förster coupled systems, it is convenient to alter γ via bias pulsing techniques [20]. It is to be noted that the cutoff frequency in equation (32) occurs at $\omega_\ell \sim \upsilon_{\mathrm{LA}}/\ell$ which is approximately the inverse phonon flight time through the quantum dot.

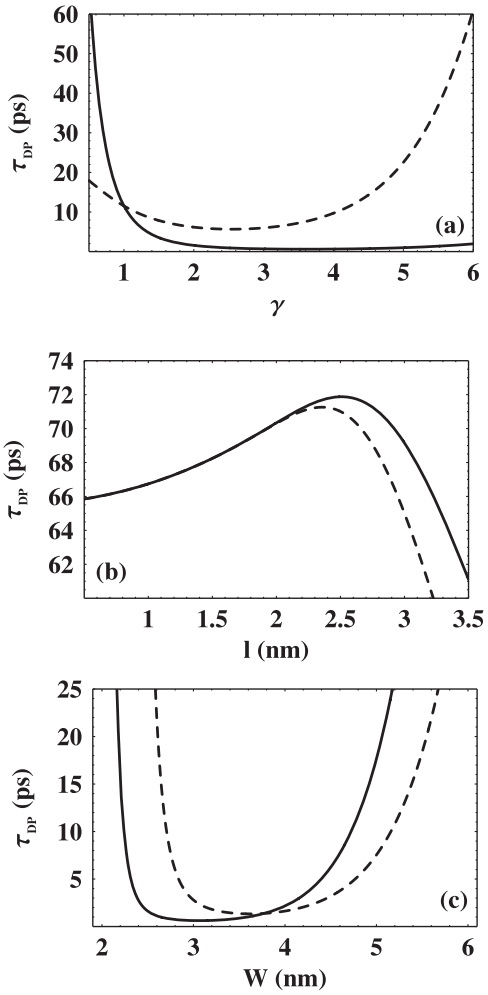

Figure 1. Relaxation time τ^r_{DP} (dashed) and dephasing time τ^p_{DP} (full) as functions of (a) $\gamma = \frac{\Delta\Omega}{2F(W)}$ at $T = 10$ K, $W = 5$ nm, $\ell_{\mathrm{e}} \approx \ell_{\mathrm{h}} = \ell = 2$ nm and $\ell_{z\mathrm{e}} \approx \ell_{z\mathrm{h}} = \ell_z = 1.5$ nm, (b) dot size ℓ at $\gamma = 1$, $W = 6$ nm, $\ell_z = 0.5$ nm and $T = 10$ K. (c) Relaxation time τ^r_{DP} as a function of interdot distance W at $\gamma = 1.5$ (dashed) and $\gamma = 0.5$ (full) at $\ell = 2$ nm, $\ell_z = 1$ nm and $T = 10$ K.

We use parameters relevant to the GaAs/AlGaAs material system [21] to calculate the relaxation time τ^r_{DP} and dephasing time τ^p_{DP}, which are shown as functions of γ in figure 1(a). For small values of γ the qubit states are close to being maximally entangled and decoherence is dominated by relaxation, as one would expect for two equally populated states. As γ increases, the difference in populations of the qubit states is enhanced and decoherence becomes increasingly dominated by a pure dephasing process. The minimum relaxation time τ^r_{m} is attained at γ_m and is given by $\tau^r_{\mathrm{m}} \approx W/2\pi\upsilon_{\mathrm{LA}}$, thus satisfying the condition in which the interdot separation matches the phonon wavevector, as discussed by Zanardi *et al* [27]. Figure 1(a) shows that equation (31) provides reliable qualitative predictions for Förster coupled excitonic qubits at small interdot tunnelling energies. These decoherence times will be compared with those estimated using Markovian Bloch–Redfield theory in section 7.

Figure 1(b) shows that for $\gamma = 1$, relaxation and dephasing times differ as the quantum dot size ℓ is increased beyond 2 nm. Figure 1(c) shows that at certain values of W, depending on γ and ℓ, relaxation times can reach very small values, of the order of several picoseconds. Hence the relaxation rate has a non-monotonic dependence on the interdot distance W for a wide range of γ values.

For the case of qubit–phonon interaction via piezoelectric coupling, we obtain relaxation and dephasing rates for $\lambda = \mathrm{LA}$ using equations (20), (30), (31):

$$\frac{1}{\tau^{r(p)}_{\mathrm{Piez}}} = \frac{\pi^2 q e^2 e_{14}^2}{2\epsilon^2 \hbar \rho \upsilon_{\mathrm{LA}}^2} \exp(-q^2\ell^2/2) \times [1 - \exp(-\tfrac{1}{4}(r^2-1)q^2\ell^2)]^2 \times G_{\mathrm{LA}}\left(\frac{q^2\ell^2 r^2}{2\left(r^2+1\right)}\right)(N_{q,\lambda}+1)S'_{r(p)}(\beta), \tag{33}$$

where $r = \ell_{\mathrm{h}}/\ell_{\mathrm{e}}$ and where we have assumed $\ell = \ell_{\mathrm{e}} = \ell_{z\mathrm{e}}$, which enables us to obtain the analytical expression shown. The function G_{LA} has the expression

$$G_{\mathrm{LA}}(x) = \frac{2x+15}{4x^3} - \frac{\sqrt{\pi}\mathrm{e}^{-x}(4x(x+3)+15)\mathrm{Erfi}\left(\sqrt{x}\right)}{8x^{7/2}}, \tag{34}$$

and S'_r and S'_p are given by

$$S'_r(\beta) = \sin^2\beta\left(1 - \frac{\sin qW}{qW}\right) + 9\cos^2\beta\,\mathrm{e}^{-\frac{W^2}{\ell^2}},$$
$$S'_p(\beta) = \cos^2\beta\left(1 - \frac{\sin qW}{qW}\right) + \frac{9}{2}\sin^2\beta\,\mathrm{e}^{-\frac{W^2}{\ell^2}}.$$

Expressions similar to equation (33) but with terms $G_{\mathrm{TA1}}(x)$ and $G_{\mathrm{TA2}}(x)$ associated with TA1 and TA2 modes are given by

$$G_{\mathrm{TA1}}(x) = \frac{3}{2x^2} - \frac{\sqrt{\pi}\mathrm{e}^{-x}(2x+3)\mathrm{Erfi}\left(\sqrt{x}\right)}{4x^{5/2}},$$
$$G_{\mathrm{TA2}}(x) = \frac{\sqrt{\pi}\mathrm{e}^{-x}(x(x(2x+5)+12)+15)\mathrm{Erfi}\left(\sqrt{x}\right)}{6x^{7/2}} - \frac{x(x+2)+15}{3x^3}.$$

Equation (33) shows that $1/\tau^{r(p)}_{\mathrm{Piez}} = 0$ when $\ell_{\mathrm{h}} = \ell_{\mathrm{e}}$ (for which $r = 1$) due to the piezoelectric coupling being a polar mechanism.

Figure 2(a) shows that dephasing due to qubits interacting with phonons via piezoelectric coupling is dominant at large values of γ ($\geqslant$2.5) while relaxation dominates at small values of γ. These features are similar to those obtained for phonon coupling via the deformation potential. The results shown in figures 2(a) and (b), as well as those obtained for the deformation potential, highlight the critical role of γ and quantum dot parameters in influencing the decoherence properties of excitonic qubit systems. Therefore the quality factor Q [13], which determines the number of charge oscillations that can be resolved within the decoherence time, can be selected using the quantum dot system configuration based on parameters ℓ, ℓ_z, r, W and T. Phonon-assisted decoherence can therefore be suppressed by careful choice of system parameters leading to higher fidelity of logic gate operations.

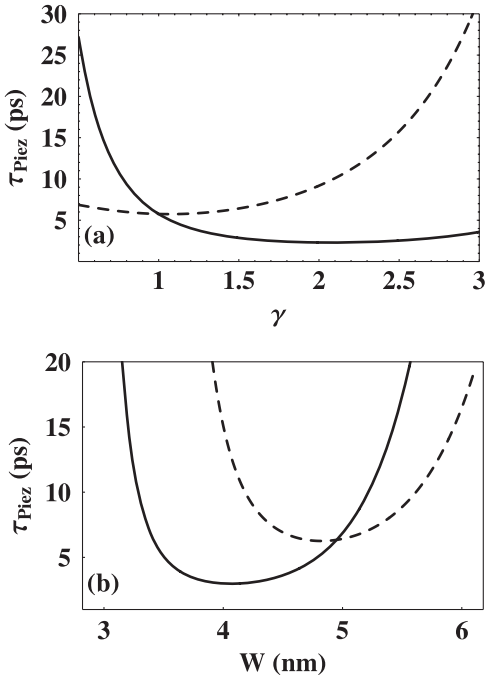

Figure 2. (a) Relaxation time τ^r_{Piez} (dashed) and dephasing time τ^p_{Piez} (full) as functions of γ at $W = 5$ nm, $\ell_{\mathrm{e}} = \ell_{z\mathrm{e}} = 2$ nm, $r = \ell_{\mathrm{h}}/\ell_{\mathrm{e}} = 5$ and $T = 10$ K. (b) Relaxation time τ^r_{Piez} as a function of interdot distance W at $\gamma = 1.5$ (dashed) and $\gamma = 0.5$ (full) at $\ell_{\mathrm{e}} = \ell_{z\mathrm{e}} = 2$ nm, $r = 5$ and $T = 10$ K.

7. Decoherence times using Markovian Bloch–Redfield theory

In this section we verify some of the results obtained in earlier sections by comparison with results of the Markovian Bloch–Redfield theory [19, 20]. For the weak damping of the qubit system and low temperature conditions considered here, the Born approximation [19, 20] becomes valid. We assume a large phonon reservoir so that the characteristic time of correlation between phonons and qubit states is less than the relaxation time of the system. This condition ensures that the system obeys the Markovian process of evolution. The Bloch–Redfield theory describes the dynamics of the two-level qubit Hamiltonian in terms of two rates: the relaxation rate and the decoherence rate [19, 20]. The pure dephasing rate is then obtained from these two rates. Analytical expressions for the decoherence ($\tau^p_{\mathrm{X,R}}$) and relaxation rates ($\tau^r_{\mathrm{X,R}}$) are given by [19, 20]

$$\frac{1}{\tau^r_{\mathrm{X,R}}} = \frac{\pi}{2}\frac{F^2}{\Delta\Omega^2 + (2F)^2} J_{\mathrm{X}}(2F)\coth\left(\frac{F}{2k_{\mathrm{B}}T}\right),$$
$$\frac{1}{\tau^p_{\mathrm{X,R}}} = 2\pi\frac{\Delta\Omega^2}{\Delta\Omega^2 + (2F)^2} G_{\mathrm{X}}(\omega\to 0), \tag{35}$$

where $X = \mathrm{DP}$ or Piez and the Förster tunnelling amplitude F depends on the interdot distance W as given in equation (14). We have $G_{\mathrm{X}}(\omega) = J_{\mathrm{X}}(\omega)\coth(\frac{\hbar\omega}{2k_{\mathrm{B}}T})$ and $J_{\mathrm{X}}(\omega)$ is the following spectral density function which yields information

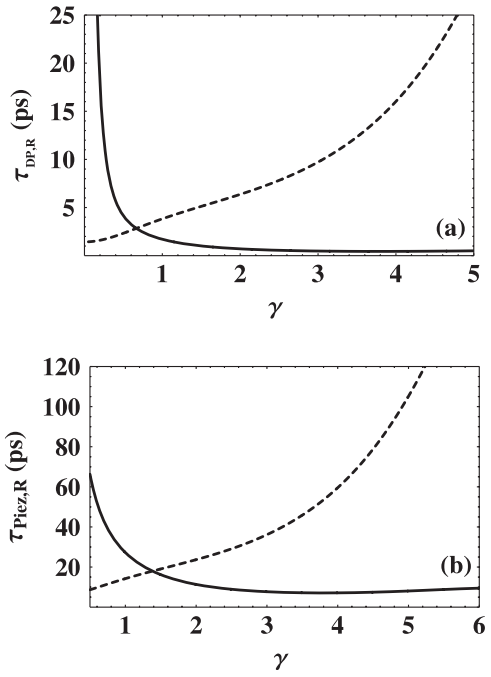

Figure 3. (a) Relaxation time $\tau^r_{\rm DP,R}$ (dashed) and dephasing time $\tau^p_{\rm DP,R}$ (full) as functions of $\gamma = \frac{\Delta\Omega}{2F(W)}$ at $T = 10$ K, $W = 5$ nm, $\ell_{\rm e} \approx \ell_{\rm h} = \ell = 2$ nm and $\ell_{ze} \approx \ell_{zh} = \ell_z = 1.5$ nm. (b) Relaxation time $\tau^r_{\rm Piez,R}$ (dashed) and dephasing time $\tau^p_{\rm Piez,R}$ (full) as functions of γ at $T = 10$ K, $W = 5$ nm, $\ell_{\rm e} \approx \ell_{ze} = 2$ nm and $r = \ell_{\rm h}/\ell_{\rm e} = 5$.

about the interaction of the quantum dot with phonons:

$$J_{\rm DP}(\omega) = \sum_q \Sigma_D(q_\parallel, q_z)^2 \delta(\omega - \omega_q)$$
$$J_{\rm Piez}(\omega, \lambda) = \sum_q \Sigma_P(q_\parallel, q_z, \lambda)^2 \delta(\omega - \omega_q), \tag{36}$$

where $\Sigma_D(q_\parallel, q_z)$ and $\Sigma_P(q_\parallel, q_z, {\rm LA})$ are given in equations (22) and (26) respectively. At small ω, $J(\omega) \sim \omega^k$ where the exponent k distinguishes the cases of ohmic ($k = 1$), sub- ($k < 1$) and super-ohmic ($k > 1$) couplings [24]. $J_D(\omega)$ and $J_P(\omega, {\rm LA})$ can be determined [25] using equations (24), (30) in super-ohmic forms where $k = 3, 5$ for $J_D(\omega)$, $J_P(\omega, {\rm LA})$ respectively.

Comparison of figures 3(a), and 1(a) shows that there is reasonable agreement (within an order of magnitude) of the decoherence times obtained using the Fermi Golden Rule and Markovian Bloch–Redfield theory for excitonic qubits interacting with acoustic phonons via the deformation potential. However we note some differences when qualitative comparisons are made especially at $0.5 \leqslant \gamma \leqslant 1$. These differences arise mainly from the restricted range of phonon frequencies involved due to the energy conservation condition of the Fermi Golden Rule formula. The energy difference between the symmetric and antisymmetric eigenstates is small, thus only low energy phonons are involved in energy conservation. This elimination process is useful in situations where the phonon bath does not have a smooth frequency distribution and for which the Markovian Bloch–Redfield theory may fail as explained in [19].

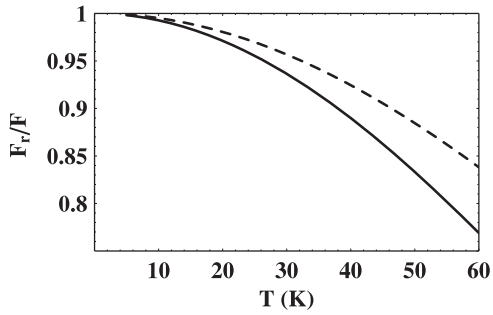

Figure 4. Renormalized tunnelling fraction $\frac{F_r}{F}$ as function of temperature at $\gamma = 1.5$ (full) and $\gamma = 1$ (dashed), $W = 6$ nm, $\ell_{\rm e} \approx \ell_{\rm h} = \ell = 2$ nm and $\ell_{ze} \approx \ell_{zh} = \ell_z = 1$ nm for the case of the deformation potential mechanism.

The Förster interaction energies are weak (≈0.4 meV) at typical interdot separations of ≈50 Å considered here and we expect the Fermi Golden Rule to provide reliable estimates of decoherence times for a wide range of parameters $(\gamma, \ell_{\rm e}, l_h, l_{ze})$. The Golden Rule employed here therefore provides a viable alternative to numerically intensive schemes [28] as equations (32) and (33) are analytically tractable and require minimum computational effort. However we have excluded very small γ values ($\leqslant$0.25) from consideration in our work as the Fermi Golden Rule contains approximations [29] that exclude vital quantum characteristics present at high interdot tunnelling amplitudes F. At such amplitudes, F becomes comparable to the cutoff frequency (see equation (32)) which occurs at $\omega_\ell \sim \upsilon_{\rm LA}/\ell$. For the GaAs/AlGaAs material system [21] typically $\omega_\ell \sim 5$ meV and we expect Markovian theories to fail at very low γ values. The resulting dynamics of qubit–phonon interactions will then need to be modelled using non-Markovian methods [30] which include phonon reservoir memory effects.

Comparing figures 3(b) and 2(a), we note that the Fermi Golden Rule also yields the correct order of magnitude for relaxation and pure dephasing times for qubits interacting with acoustic phonons via piezoelectric coupling. The qualitative deviations are however more marked in this case possibly due to the nature of the spectral density function associated with the piezoelectric mechanism.

7.1. Renormalized tunnelling amplitude F_r

Due to phonon interactions the interdot tunnelling amplitude F (see equation (14)) gets dressed by a Franck–Cordon (FC) factor and the renormalized amplitude $F_{\rm r}$ is modified [25] according to

$$F_{\rm r} = F \exp\left[-\int_0^\infty \frac{J_{\rm X}(\omega)}{\omega^2} \coth\left(\frac{\hbar\omega}{2k_{\rm B}T}\right) {\rm d}\omega\right].$$

The argument of the exponential term in $F_{\rm r}$, the FC factor [25], is computed using the spectral density functions given in equation (36). For the GaAs/AlGaAs material system [21], the renormalized tunnelling amplitude $F_{\rm r}$ (plotted in figure 4) is only marginally affected in the low temperature range ($T \leqslant$ 50 K) which we have considered in our work. This justifies the exclusion of the FC factor in estimating decoherence

times in section 6. It is important to note that the degree of renormalization of the interdot tunnelling amplitude F increases as γ is increased.

8. Conclusions

We have studied phonon-assisted mechanisms that contribute to the decoherence of excitonic qubits in quantum dot systems coupled by Förster-type transfer. We have obtained explicit expressions for the relaxation and dephasing times of excitonic qubits interacting with acoustic phonons that are valid at small interdot tunnelling energies. Our results highlight the critical role of the bias in influencing the decoherence properties of excitonic qubit systems. For instance, increasing the tuning factor γ has opposite effects on the relaxation and dephasing times for excitonic qubits. Numerical estimates of decoherence times using Markovian Bloch–Redfield theory agree within an order of magnitude with times obtained using the Fermi Golden Rule in GaAs/AlGaAs quantum dot systems for $\gamma \geqslant 0.5$. The Fermi Golden Rule therefore provides a viable alternative to numerically intensive schemes at interdot tunnelling amplitudes small enough for Markovian theories to be valid. We note that generic features of decoherence of excitonic qubits are essentially the same for phonons which interact via both the deformation potential and piezoelectric coupling.

References

[1] Loss D and DiVincenzo D P 1998 *Phys. Rev.* A **57** 120–6
[2] Biolatti E, Iotti R C, Zanardi P and Rossi F 2000 *Phys. Rev. Lett.* **85** 5647–50
[3] Li X, Wu Y, Steel D, Gammon D, Stievater T H, Katzer D S, Park D, Piermarocchi C and Sham L J 2003 *Science* **301** 809–11
[4] Krenner H J, Stufler S, Sabathil M, Clark E C, Ester P, Bichler M, Abstreiter G, Finley J J and Zrenner A 2005 *New J. Phys.* **7** 184
[5] Muller A, Wang Q Q, Bianucci P, Shih C K and Xue Q K 2004 *Appl. Phys. Lett.* **84** 981–3
[6] Zrenner A, Beham E, Stufler S, Findeis F, Bichler M and Abstreiter G 2002 *Nature* **418** 612–4
[7] Lovett B W, Reina J H, Nazir A and Briggs G A D 2003 *Phys. Rev.* B **68** 205319
[8] Nazir A, Lovett B W and Briggs G A D 2004 *Phys. Rev.* A **70** 052301
[9] Nazir A, Lovett B W, Barrett S D, Reina J H and Briggs G A D 2005 *Phys. Rev.* B **71** 045334
[10] Förster T 1948 *Ann. Phys., Lpz.* **2** 55–75
[11] Dexter D L 1953 *J. Chem. Phys.* **21** 836–50
[12] Zanardi P and Rasetti M 1997 *Phys. Rev. Lett.* **79** 3306–9
[13] Hohenester U 2006 *Phys. Rev.* B **74** 161307(R)
[14] Xue P and Xiao Y-F 2006 *Phys. Rev. Lett.* **97** 140501
[15] Takagahara T 1993 *Phys. Rev. Lett.* **71** 3577–80
[16] Fedichkin L and Fedorov A 2004 *Phys. Rev.* A **69** 032311
[17] Hayashi T, Fujisawa T, Cheong H D, Jeong Y H and Hirayama Y 2003 *Phys. Rev. Lett.* **91** 226804
[18] Jacak L, Hawrylak P and Wojs A 1998 *Quantum Dots* (Berlin: Springer)
[19] Weiss U 1999 *Quantum Dissipative Systems* 2nd edn (Singapore: World Scientific)
[20] Vorojtsov S, Mucciolo E R and Baranger H U 2005 *Phys. Rev.* B **71** 205322
[21] Thilagam A and Lohe M A 2006 *J. Phys.: Condens. Matter* **18** 3157–77
[22] Franceschetti A and Zunger A 1997 *Phys. Rev. Lett.* **78** 915–8
[23] Allan G and Delerue C 2007 *Phys. Rev.* B **75** 195311
[24] Krummheuer B, Axt V M and Kuhn T 2002 *Phys. Rev.* B **65** 195313
[25] Leggett A J, Chakravarty S, Dorsey A T, Fisher M P A, Garg A and Zwerger W 1987 *Rev. Mod. Phys.* **59** 1–85
[26] Merzbacher E 1970 *Quantum Mechanics* (New York: Wiley)
[27] Zanardi P and Rossi F 1998 *Phys. Rev. Lett.* **81** 4752–5
[28] Thorwart M, Paladino E and Grifoni M 2004 *Chem. Phys.* **296** 333–44
[29] Fiori E R and Pastawski H M 2006 *Chem. Phys. Lett.* **420** 35–41
[30] Maniscalco S 2007 *Phys. Rev.* A **75** 062103